MARKER TRACKS POST-PROCESSING FOR ACCURATE FIDUCIAL MARKER POSITION ESTIMATION IN CONE BEAM CT PROJECTION IMAGES

Bogdan Matuszewski

School of Computing Engineering and Physical Sciences, University of Central Lancashire, Preston, U.K.

Tom Marchant

North Western Medical Physics, The Christie NHS Foundation Trust, Manchester, U.K.

Andrzej Skalski

Department of Measurment and Instrumentation, AGH University of Science and Technology, Kraków, Poland

Keywords: Fiducial marker tracking, Cone beam CT, Combinatorial optimisation.

Abstract: This paper describes details of a method for robust and accurate marker position estimation in projection CB images. The method is based on previously proposed tracking algorithms which can cope with multiple proximate markers and image clutter. The algorithm described in this paper can be seen as a post processing algorithm which uses all the calculated hypothetical marker positions, from the tracking algorithm, for all the markers and all projection images in a single combinatorial optimisation process. The algorithm has been design to estimate intra fraction motion during image guided radiation therapy. The results from the algorithm can be used in treatment planning, subsequent treatment monitoring and correction of motion artefacts in cone beam CT. The proposed post processing algorithm reduced the maximum marker position error from 5.6 pixels, using tracker alone, to 2.6 pixels after post processing. This should be compared to estimated 2.5 pixels maximum error present in the ground truth data. For the total number of 3,840 tracked markers after post processing 1.61% and 0.02% of their positional errors were respectively above three and six standard deviation of the ground truth, estimated separately for each marker and each projection image, whereas corresponding results after using tracker alone were 2.86% and 0.23%.

1 INTRODUCTION

Radiation therapy exploits the extra susceptibility of many cancers to repeated insult by radiation compared to healthy tissues. The radiation beams are applied sequentially to a target volume from different directions in a manner pre-determined by computerised dosimetric planning. The treatments are commonly divided into daily fractions delivered over several weeks. Because of uncertainties, including tumour motion, a safety margin is added around the clinical target volume (CTV) leading to a bigger planning target volume (PTV).

Tumour tracking is an important tool in modern radiotherapy, as it is instrumental in measurement of tumour intra fraction motions enabling a variety of strategies for management of motion in radiotherapy. More specifically it is important in solving such tasks as treatment planning, patient position monitoring, gating, and CBCT volume reconstruction with motion corrections.

There are a number of techniques being developed for tumour tracking which avoid additional ionising radiation delivered to the patient, including: MV portal image tracking (Keall *et al* 2004), electromagnetic markers (Willoughby *et al* 2006), optical surface sensing (Moore and Graham 2000, Hoisak *et al* 2004). However, the technique becoming most widely available in clinical practice is using one or more pairs of kV x-ray tubes and imagers integrated with the MV x-ray treatment

machine (Balter and Cao 2007). Such devices provide information about local anatomy in the form of fluoroscopic images and/or cone beam CT (CBCT), enabling tracking and measurement of tumour motion (Shirato *et al* 1999, Marchant *et al* 2008, Poulsen *et al* 2008).

There are essentially two methodologies for tracking tumours in the kV images. The first is using directly the image intensity patterns to estimate tumour mass position without any implanted markers (Cui *et al* 2007) but this approach however is still considered to be under development. The second methodology tracks one or more implanted radio-opaque fiducial markers which are treated as a reliable tumour surrogate. The RTRT (Shirato *et al* 1999) and IRIS (Berbeco *et al* 2004) are examples of the hardware platforms proposed to solve this problem. Both these systems use multiple pairs of diagnostic x-ray tubes and imagers to determine the 3D marker position. The RTRT system uses a simple template matching tracking algorithm to track a single spherical marker. Tang *et al* (2007) proposed a tracking algorithm capable of tracking multiple cylindrical markers in fluoroscopic images acquired from a monoscopic system. Their method uses template matching in conjunction with a prediction stage and multiple hypotheses to improve robustness of the tracker in a presence of image clutter. More recently Matuszewski *et al* (2010) proposed tracking algorithm with multi-component score functions to select the most likely position of the marker from a set of generated marker position hypotheses. In comparison to the algorithm proposed in (Tang *et al* 2007) the method uses: (i) the mean shift algorithm instead of template matching, which provides higher accuracy due to explicit sub-pixel accuracy of marker position estimation and dynamic implicit estimation of markers appearance (ii) use of random sampling for hypothesis generation instead of deterministic evaluation of all possible marker locations in the predefined size window, enabling efficient marker search in a much bigger region, and maintaining track of possibly widely spatially separated positional hypotheses. Additionally contrary to the method described in (Tang *et al* 2007) the method proposed in (Matuszewski *et al* 2010) can operate even when: (i) average intensity of the markers changes significantly; (ii) apparent marker shape changes significantly; (iii) the breathing pattern changes. The method does not assume posterior distribution to be Gaussian, indeed due to image clutter and presence of other proximate markers the likelihood function could be highly non-Gaussian – with multiple significant modes.

The method described in this paper can be seen as an extension of the method proposed in (Matuszewski *et al* 2010) where all the marker position hypothesis are used in a batch processing mode in a single combinatorial optimisation process.

The batch processing rather than real-time tracking can be justified for some applications, for example in CBCT motion correction. The tracking of fiducial markers in such data is a challenging problem. There are a number of reasons for this including: a high level of noise due to scatter and a low radiation dose delivered during a single CB projection image acquisition; markers changing shape and size for different projection angles; occlusions and clutter caused by possible presence of the foreign objects; markers overlapping with each other or being masked by anatomical structures; significant variations of the marker and background intensities with projection angle. Additionally apparent marker displacement in two consecutive images could be quite significant as it is a superposition of an intrinsic motion caused, for example, by respiration and an extrinsic motion induced by the sensor rotation.

The rest of the paper is organised as follows: in section 2 the cone beam CT projection images are introduced, section 3 briefly summarises the algorithm proposed in (Matuszewski *et al* 2010), whereas section 4 describes in details proposed extensions of the method. The experimental results are presented in section 5 with conclusions drawn in section 6.

2 CONE BEAM CT PROJECTION IMAGES

CB projection images shown in this paper were acquired using Electra Synergy (XVI 3.5, Elekta, Crawley, UK). This system has a kV imager fixed to the rotating gantry, mounted orthogonally to the MV treatment beam. Projection images were captured over 360° of rotation at a frame rate of 5.5Hz with 640 projections. Projection images were acquired using a 512x512 matrix with square pixel of size $s = 0.8$ mm at the detector. The geometrical configuration of the rotating gantry with kV and MV sources and kV imager is shown in Figure 1.

Assuming that the position (x,y,z) of a marker in 3D space is fixed its apparent motion in the projection images as a function of the gantry angle is given by (Marchant 2008):
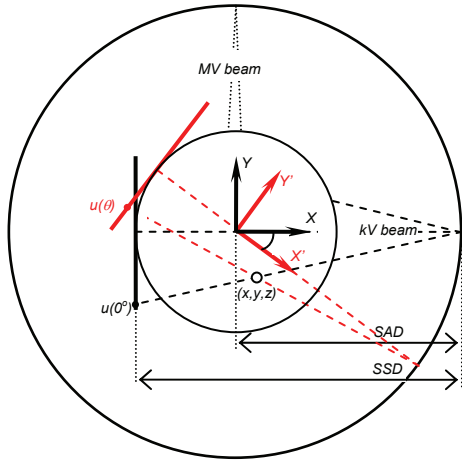
Figure 1: Geometry of the CB imaging system.

$$u(\theta) = \frac{SDD}{s} \times \frac{\sin(\theta)x + \cos(\theta)y}{SAD - (\cos(\theta)x - \sin(\theta)y)} + o_u$$

$$v(\theta) = \frac{SDD}{s} \times \frac{z}{SAD - (\cos(\theta)x - \sin(\theta)y)} + o_v \quad (1)$$

Where $u(\theta)$ and $v(\theta)$ are respectively row and column coordinates of the marker in the projection image acquired at θ gantry angle, o_u and o_v represent the position of the principal point in the image coordinates; θ is the known gantry rotation angle, *SDD* and *SAD* are the known distances from the source to the detector and gantry rotation axis respectively. The apparent 2D motion of the marker in the sequence of projection images is a superposition of the motion induced by the rotating gantry and the motion due to 3D marker movement.

The apparent marker motion in the projection images due to the gantry rotation and the actual marker displacement in 3D space can be separated by fitting functions $u(\theta)$ and $v(\theta)$ given in (1) to the observed marker positions $\left(v_k^m, u_k^m\right)$ in the projection images, with *k* and *m* indexes identifying projection image and marker respectively. This has been implemented using the Levenberg-Marquardt method to optimise a nonlinear least squares cost function. As the result of this procedure for each marker, *m*, vector $\left(\bar{x}^m, \bar{y}^m, \bar{z}^m\right)$ is estimated representing its mean position in the 3D space.

The method was tested using projections from CBCT image of a pancreatic cancer patient. The patient had six gold seeds (fiducial markers) each size of 1mm × 10mm placed into the pancreas at surgery prior to radiotherapy. Figure 2 shows sample CB projection images acquired for different gantry rotation angles, illustrating changes in signal level

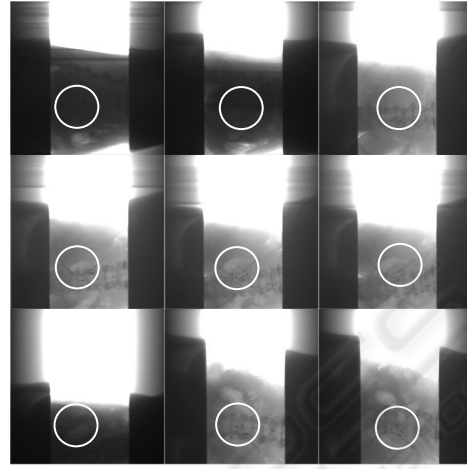and contrast, with location of the markers indicated by white circles.

Figure 2: Sample of CB projection images acquired with different gantry rotation angle.

3 MARKER TRACKING

As it was explained in the introduction tracking fiducial markers in the CB projection images is a challenging problem. To tackle this problems effectively and robustly Matuszewski *et al* (2010) proposed tracking algorithm which brings together prior knowledge about the apparent motion of the markers in the CB image sequence with a hybrid tracking algorithm combining mean shift (Comaniciu and Meer 2002) and particle filter (Doucet *et al* 2001, Arulampalam *et al* 2002) methodologies. At initialisation the position of all the *M* markers $\left\{x_0^m; m = 1 \ldots M\right\}$ are selected manually in the first CB projection image. The positions of the corresponding markers in the subsequent projection images are estimated (tracked) using probabilistic framework where the position $x_k^m = \left(v_k^m, u_k^m\right)^T$ of marker *m* at image *k* given all observations $z_{1:k}$ till current image is given in terms of posterior probability $p\left(x_k^m | z_{1:k}\right)$ and the tracking consist of two interleaving steps of prediction and update. During the prediction step the position of the marker in the next frame $p\left(x_{k+1}^m | z_{1:k}\right)$ is calculated based on the estimated position in the current frame, a dynamic model of motion consisting of a deterministic propagation model and a stochastic perturbation model. In the update state the new

observations z_{k+1} are used to refine the marker position using measurements $p\left(z_{k+1}\middle|x^m_{k+1}\right)$ in the Bayesian formula

$$p\left(x^m_{k+1}\middle|z_{1:k+1}\right) \propto p\left(z_{1:k+1}\middle|x^m_{k+1}\right)p\left(x^m_{k+1}\middle|z_{1:k}\right) \qquad (2)$$

Due to the previously mentioned clutter and occlusions in the projection images $p\left(x^m_k\middle|z_{1:k}\right)$ could be highly non-Gaussian with multiple significant modes. This prevents the use of standard Kalman Filter or Extended Kalman Filter trackers. Instead a particle filter tracker is used where the posterior is approximated by a discrete set of particles $\left\{x^{m,i}_k; i=1\ldots N\right\}$ (samples from the posterior distributions) and the corresponding weights $\left\{\pi^{m,i}_k; i=1\ldots N\right\}$ corresponding to probabilities of drawing corresponding particles:

$$p\left(x^m_k\middle|z_k\right) \propto \sum_{i=1}^{N} \pi^{m,i}_k \cdot \delta\left(x^m_k - x^{m,i}_k\right) \qquad (3)$$

The position of the marker is estimated based on the posterior using maximum a posteriori probability approach (MAP). The main modifications to the particle filter proposed used for the tracking of fiducial markers in the sequence of CB projection images include use of equations of apparent motion of the markers due to rotation of the gantry and introduction of the mean shift in the prediction stage. The use of the mean shift has a twofold effect. Firstly it significantly reduces the number of particles necessary for representing the posterior as in this case all the particles would represent main modes of the posterior. In fact the number of particles can vary between different images. If there are no occlusions or clutter there may be a single particle propagating to the next frame, describing the position of the mode of the uni-modal posterior distribution. If there is significant clutter in the image more particles will be used to describe the multimodal posterior distribution. Secondly it provides more accurate MAP estimates as the mean shift algorithm guarantees convergence to, at least, local maxima of the posterior, whereas the original particle filter only randomly samples from the posterior and as such the location of the maximum of the posterior may not be represented in the drawn particles. In most cases this scheme provides accurate tracking results. In some cases where markers come very closely together or indeed overlap in the projection images the tracking accuracy may drop and in some cases the identity of

the markers might be confused. By the tracker design when markers move apart the tracker is able to recover correct marker identity and resume tracking with normal accuracy. For some applications, for example CB volume reconstruction (Marchant *et al* 2009), real-time tracking is not necessary as the data may be processed after acquisition of all projection images is complete. In this case results can be improved further by batch post-processing of the data. In the post processing algorithm proposed in this paper all the particles $x^{m,i}_k$ generated for all the markers *m*, and all images *k* are fed to a function which assigns a cost to all possible track configurations supported by the drawn particles. The configuration of particles with the lowest cost function defines final estimate of the markers' positions.

4 MARKER TRACKS POST PROCESSING

The tracking method introduced in the previous section generates particles (hypotheses) for the estimated marker's position. The number of these particles depends on the local image complexity. This may include image clutter, and/or presence of other markers being close or indeed overlapping with the marker for which position is estimated. For complex configurations the tracker can generate tens of hypothetical positions for each marker, or just a single one if there is no image clutter or other adjacent markers. To evaluate the quality of the generated particles it is proposed to calculate for each particle a score based on a number of criteria, assessing how well the given prediction describes the prior knowledge about the marker. This is aiming at improving estimation accuracy and helping to recover from possible track losses. The score function adopted in this paper is defined as:

$$s\left(x^{m,i}_k\right) = \alpha_{Ms} s_{Ms}\left(x^{m,i}_k\right) + \alpha_{Mu} s_{Mu}\left(x^{m,i}_k\right) + \\ \alpha_{Mv} s_{Mv}\left(x^{m,i}_k\right) + \alpha_{Ds} s_{Ds}\left(x^{m,i}_k\right) \qquad (4)$$

And the final estimate $\hat{x}^m_k$ of the *m*th marker position is given as:

$$\hat{x}^m_k = x^{m,\hat{i}}_k, \quad \hat{i} = \arg\max_i s\left(x^{m,i}_k\right) \qquad (5)$$

where: $x^{m,i}_k = \left(v^{m,i}_k, u^{m,i}_k\right)$ is *i*-th position prediction for *m*-th marker in the *k*-th image; $s_{Ms}\left(x^{m,i}_k\right)$, $s_{Mu}\left(x^{m,i}_k\right)$,

$s_{Mv}\left(x_k^{m,i}\right)$, and $s_{Ds}\left(x_k^{m,i}\right)$ are respectively mode similarity measure, u- and v-coordinate prediction measures, and distance measure to the closest marker, described below.

Mode similarity measure is directly obtained from the mean shift algorithm. It indicates how strongly the intensity pattern around the predicted position (mode location) reflects the expected marker shape and orientation. It is defined as:

$$s_{Ms}\left(x_k^{m,i}\right) = \frac{\sum_{l=1}^{n} w(x_l) g_{\Sigma_m}\left(x_k^{m,i} - x_l\right)}{\max_j \sum_{l=1}^{n} w(x_l) g_{\Sigma_m}\left(x_k^{m,j} - x_l\right)} \quad (6)$$

where: g_{Σ_m} is Gaussian kernel with covariance matrix Σ_m; $w(x_l)$ represents the image intensities. The estimated marker size and orientation in the projection image, encoded by the kernel's covariance matrix Σ_m, is updated in each image as long as there is no clutter in the proximity of marker m.

u-coordinate prediction measure penalises (assigns low score values to) predicted marker positions for which the error between their u-coordinates and the corresponding model prediction $u^m(\theta_k)$ differs significantly from what is expected. Based on experimental analysis $s_{Mu}\left(x_k^{m,i}\right)$ is modelled as having the Gaussian distribution with mean value of $\hat{u}^m(\theta_k)$ calculated from (1) using all position estimates $\left\{n : \hat{u}_n^m = u_n^{m,i}\big|_{i=\{1\}}\right\}$ with only one particle (indicating uni-modal probability distribution), and the dispersion σ_u set as one of the method design parameters:

$$s_{Mu}\left(x_k^{m,i}\right) = \mathcal{N}\left(u_k^{m,i}\big|\hat{u}^m(\theta_k), \sigma_u\right) \quad (7)$$

v-coordinate prediction measure, weighs v-coordinate of the predicted marker position $v_k^{m,i}$ with respect to the corresponding coordinate $\hat{v}_{k-1}^m$ estimated for the previous frame. This prediction error is modelled using a Gaussian distribution with a mean value of $\Delta v_k^{-m,\{N\}}$ and dispersions $\sigma_{v,card\{N\}}$ defined as the method design parameters:

$$s_{Mv}\left(x_k^{m,i}\right) = \mathcal{N}\left(v_k^{m,i} - \hat{v}_{k-1}^m\big|\Delta v_k^{-m,\{N\}}, \sigma_{v,card\{N\}}\right) (8)$$

where: $\Delta v_k^{-m,\{N\}}$ is an estimated displacement of marker m, used to predict its v-position in the k image, calculated as the mean from the displacement calculated for all the other reliable markers (markers described by a uni-modal distribution):

$$\Delta v_k^{-m,\{N\}} = \frac{1}{card\{N\}} \sum_{\substack{j \in \{N\} \\ m \notin \{N\}}} \left(\hat{v}_{k+1}^j - \hat{v}_k^j\right) \quad (9)$$

with $\{N\}$ representing the set of indexes of markers described by a uni-modal distribution in frame k-1; model dispersion $\sigma_{v,card\{N\}}$ is the method design parameter, which depends on number $card\{N\}$ of reliable markers in frame k-1.
$s_{Mv}\left(x_k^{m,i}\right)$ is used in the score function only if there is at least a single marker from which $\Delta v_k^{-m,\{N\}}$ can be calculated.

Distance measure to the closest marker, is used to "encourage" separation of the overlapping markers. Without this component, on some occasions when markers are crossing each other, the estimated positions for two or more markers can be assigned to the marker which is better defined in the image. This component has only local influence as the u-direction prediction quality measure would dominate when the markers are becoming significantly separated in u-direction, and therefore this is only used when $\min_{n \neq m;j}\left(\left\|x_k^{m,i} - x_k^{n,j}\right\|\right)$ is smaller than a predefined threshold value.

$$s_{Ds}\left(x_k^{m,i}\right) = \frac{\min_{n \neq m;j}\left(\left\|x_k^{m,i} - x_k^{n,j}\right\|\right)}{\max_{n \neq m;i;j}\left(\left\|x_k^{m,i} - x_k^{n,j}\right\|\right)} \quad (10)$$

Corresponding weighting parameters α_{Ms}, α_{Mu}, α_{Mv}, α_{Ds} are problem dependent and are selected so $\alpha_{Ms} + \alpha_{Mu} + \alpha_{Mv} + \alpha_{Ds} = 1$.

Although the processing stages described so far constitute a complete tracking algorithm, the performance can be improved by batch post-processing. The post-processing proposed in this paper uses all the available $x_k^{m,i}$ from the tracking algorithm in the batch processing mode. The main objective of this post- processing step is to correct possible mistakes in the estimated marker positions when markers appear very closely in the images as the proposed tracking algorithm can "confuse" their

identity. When markers move further apart, the algorithm eventually recovers and tracks markers correctly as the previously described score function forces the tracker to reassign correct marker identities. There are two basic ideas behind proposed post processing. Firstly; to use motion models $u^m(\theta)$ calculated for all markers m estimated using all reliable marker positions and thereby enabling higher accuracy of parameter estimation in the $u^m(\theta)$ models. Secondly; to replace multiple trackers using multiple score functions with a single tracker using a single score function to assign the best marker position configuration as a result of a single optimisation process. Assuming that set $\{M\}$ represents markers which are close in image k as estimated from the models $u^m(\theta_k)$, for each $m \in \{M\}$ the proposed post-processing algorithm uses all $x_k^{m,i}$, as defined in previous section. Assuming that indexes of the M close markers are denoted by $i_1,...,i_M$ and for each of these markers there are $K_{i_1},...,K_{i_M}$ predicted positions from the mean shift mode seeking stage the cost function will evaluate all $\prod_{n=1}^{M} K_{i_n}$ combinations of the form $\left\{ x_k^{i_1,j_1},...,x_k^{i_M,j_M} \right\}$ where $j_n = 1,...,K_{i_n}$. In this new score function $S\left(x_k^{i_1,j_1},...,x_k^{i_M,j_M} \right)$ component $s_{Ds}\left(x_k^{m,i} \right)$ from equation 9 is replaced with the score component which penalises any disparity between $\left(u_k^{i_m,j_m} - u_k^{i_n,j_n} \right)$ and $\left(u^{i_m}(\theta_k) - u^{i_n}(\theta_k) \right)$ calculated pair wise, where $\{m,n\} \in C_2^{\{i_1,...,i_M\}}$ (all 2 element combinations from the set $\{i_1,...,i_M\}$ of M elements).

5 EXPERIMENTAL RESULTS

To help with the development of the algorithm as well as to provide means for algorithm validation ground truth data was gathered first. The ground truth data describes the position, of the marker mid-point, for each marker in each projection image. It was calculated as an arithmetic mean from three manual measurements taken by three different observers. The quality of this data has been assessed using the standard deviation calculated for each

marker and each image. The information about the precision of the ground truth data is subsequently used in quantitative evaluation of the proposed method. Figure 3 shows an example of three images from the sequence of CB projection images. In these images the ground truth markers' positions are shown by circles and the corresponding estimated marker positions by crosses, with the corresponding particles represented by squares. These images show an example when two of the markers (on the left of the image) are getting closer till they completely overlap, subsequently markers separate but the proposed algorithm is able to maintain correct identity of the markers. The images also show that for isolated markers only one particle is maintained as the probability density function describing their position is uni-modal.
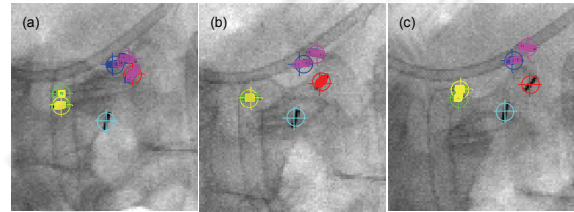

Figure 3: Images showing tracking results for overlapping markers.

Figure 4 shows the difference (red line) between estimated, using the tracking method described in section 3, and ground truth position as a function of the gantry rotation angle for three randomly selected markers. For reference standard deviation limits $\pm\sigma$ and $\pm3\sigma$ for the ground truth are also shown as blue and green lines respectively. The ground truth standard deviation changes significantly from one image to another as it is estimated from only three measurements per marker. To reduce this effect the dispersion was filtered by a moving average filter and used subsequently in the method evaluation. The filtered version of the $\pm3\sigma$ is shown as magenta coloured lines. As seen most of the error is within or close to $\pm3\sigma$ of the ground truth apart from a few spikes caused by temporal errors in marker identity estimation. Figure 5 shows the same information as in figure 4 but after post-processing as described in section 4. It can be seen that the error spikes caused by marker identity estimation error are eliminated and indeed for most of the time the markers' position is estimated within $\pm\sigma$ of the ground truth marker position. After applying proposed post processing the maximum marker position error was estimated at 2.59 pixels compared to 2.51 pixels for the ground truth and 5.6 pixels for tracking without
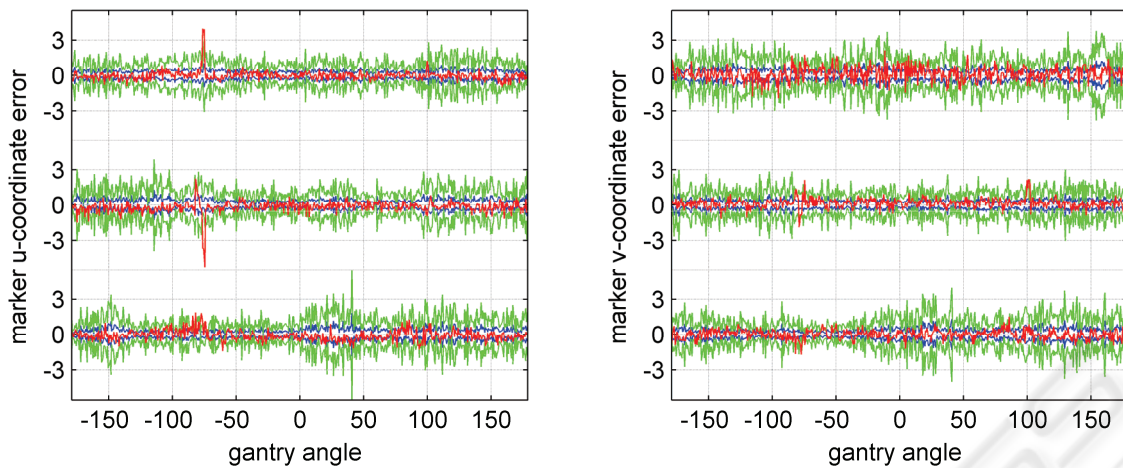
Figure 4. Error between estimated marker position and the corresponding ground truth position obtained for the tracking algorithm described in section 3.
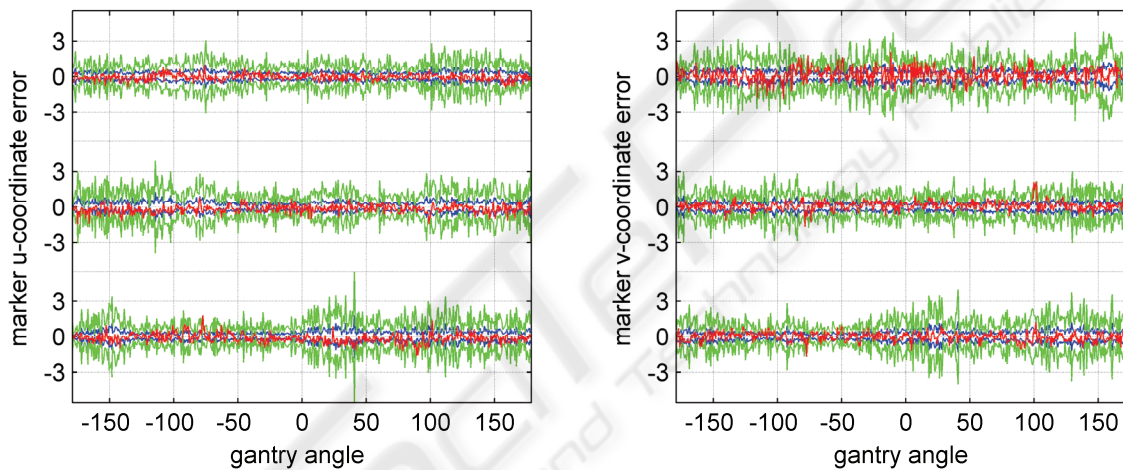

Figure 5. Error defined as in figure 4 obtained after applying proposed post-processing described in section 4.

post processing. The average standard deviation was estimated at 0.42 pixels compared to 0.44 for the ground truth and 0.47 pixels without post processing. For the total number of 3,840 tracked markers after post processing 1.61% and 0.02% of their positional errors were respectively above three and six standard deviation of the ground truth, estimated separately for each marker and each projection image, whereas corresponding results without post processing where 2.86% and 0.23%.

6 CONCLUSIONS

The paper describes in detail a modification to previously proposed automatic fiducial marker tracking algorithm. The proposed modifications require batch processing of all the available measurement but as result improve the robustness and accuracy of markers' position estimates. The proposed method uses a combination of the mean shift algorithm, sequential random sampling, custom designed constraints, and combinatorial optimisation. The tests show that the accuracy and robustness of the proposed method is superior to the results obtained by human observers. The method was specifically developed for CBCT projection images for correction of motion artefacts in the reconstructed 3D CBCT volume.

REFERENCES

Arulampalam S, Maskell S, Gordon N and Clapp T 2002
A tutorial on particle filters for on-line non-linear/non-Gaussian Bayesian tracking, *IEEE Transactions on Signal Processing* 50 174-188

Balter J M and Cao Y. 2007 Advanced technologies in image-guided radiation therapy *Semin. Radiat. Oncol.* 17 293-297

Berbeco R I, Jiang S B, Sharp G C, Chen C T Y, Mostafi H and Shirato H 2004 Integrated radiotherapy imaging system (IRIS): design considerations of tumour tracking with linac gantry-mounted diagnostic x-ray system with flat-panel detectors *Phys. Med. Biol.* 49 243-55

Comaniciu D and Meer P 2002 Mean Shift: A robust approach towards feature space analysis *IEEE Trans. Pattern Analysis and Machine Intelligence* 24 603-19

Cui Y, Dy J G, Sharp G C, Alexander B and Jiang S B 2007 Robust fluoroscopic respiratory gating for lung cancer radiotherapy without implanted fiducial markers *Phys. Med. Biol.* 52 741-55

Doucet A, Freitas N, Gordon N 2001 *Sequential Monte Carlo Methods in Practice* (New York: Springer)

Hoisak J D P, Sixel K E, Tirona R, Cheung P C F and Pibnol J P 2004 Correlation of lung tumor motion with external surrogate indicators of respiration *Int. J. Radiat. Oncol. Biol. Phys.* 60 1298-306

Keall P J, Todor A D, Vedam S S, Bartee C L, Siebers J V, Kini V R and Mohan R 2004 On the use of EPID-based implanted marker tracking for 4D radiotherapy *Med. Phys.* 31 3492-9

Marchant T E, Amer A M and Moore C J 2008 Measurement of inter and intra fraction organ motion in radiotherapy using cone beam CT projection images *Phys. Med. Biol.* 53 pp. 1-12

Marchant T, Price G, and Moore C, 2009, 'Motion Correction in Cone Beam CT (CBCT) by Projection Image Warping', UK Radiation Oncology Conference, Cardiff, 6-8 April 2009 (abstracted in Clinical Oncology 21 (3) p243). DOI: 10.1016/j.clon.2009.01.001

Matuszewski B J Skalski A, Marchant T E, 2010, Automatic tracking of implanted fiducial markers in cone beam CT projection images, submitted to *Physics in Medicine and Biology.*

Moore C J and Graham P A 2000 3D dynamic body surface sensing and CT-body matching a tool for patient set-up and monitoring in radiotherapy, *J. Computer Aided Surgery*, Special Edition on Planning and Image-Guidance in Radiation Therapy 5 2000 234-45

Poulsen P R, Cho B and Keall P J 2008 A method to estimate mean position, motion magnitude, motion correlation, and trajectory of a tumor from cone-beam CT projections for image-guided radiotherapy *Int. J. Radiation Oncology Biol. Phys.* 72 1587-1596

Shirato H, Shimizu S, Shimizu T, Kitamura K, Nishioka T, Kagei K, Hashimoto S, Aoyama H, Kunieda T, Shinohara N, Dosaka-Akita H and Miyasaka K 1999 Four-dimensional treatment planning and fluoroscopic real-time tumor tracking radiotherapy for moving tumor *Int. J. Radiat. Oncol. Biol. Phys.* 48 435-42

Tang X, Sharp G C and Jiang S B 2007 Fluoroscopic tracking of multiple implanted fiducial markers using multiple object tracking *Phys. Med. Bio* 52 4081-98

Willoughby T R, Kupelian P A, Pouliot J, Shinohara K, Aubin M, Roach M, Skrumeda L L, Balter J M, Litzenberg D W Hadley S W, Wei J T and Sandler H M 2006 Target localization and real-time tracking using the Calypso 4D localization system in patients with localized prostate cancer, *Int J radiat Oncal Biol Phys* 65 528-34